Geophysical Journal International

Geophys. J. Int. (2022) **230,** 2056–2072
Advance Access publication 2022 April 23
GJI Seismology

https://doi.org/10.1093/gji/ggac157

A first 3-D shear wave velocity model of the Ischia Island (Italy) by HVSR inversion

Roberto Manzo [1,2] Lucia Nardone [2] Guido Gaudiosi,[2] Claudio Martino,[2] Danilo Galluzzo,[2] Francesca Bianco[2] and Rosa Di Maio[1]

[1] *Dipartimento di Scienze della Terra, dell'Ambiente e delle Risorse, Università di Napoli Federico II,* 80126 *Napoli NA, Italy. E-mail: roberto.manzo@unina.it*

[2] *Istituto Nazionale di Geofisica e Vulcanologia, Sez. di Napoli, Osservatorio Vesuviano,* 80125 *Naples, Italy*

Accepted 2022 April 19. Received 2022 April 11; in original form 2021 June 28

SUMMARY

Following the M_w 3.9 earthquake that occurred in the Ischia island (Naples, southern Italy) on 21 August 2017, the local monitoring seismic network was significantly improved in terms of both number of stations and instrumentation performance. Due to the huge amount of collected seismic ambient noise data, in this paper we present a first 3-D shear wave velocity model of the island retrieved from the inversion of horizontal-to-vertical spectral ratio curves by fixing the shear wave velocities (*Vs*) and modifying the thicknesses to get the corresponding 1-D *Vs* models. We are confident about the robustness of the attained models since the inversion process provided a good convergence towards the best-fitting solutions. Then, a first 3-D velocity model was obtained by contouring all the 1-D models obtained for the selected seismic stations to highlight possible lateral variations of the layer thicknesses and to reconstruct the morphology of the deeper interface characterized by a high-impedance contrast. A good correspondence between the 3-D *Vs* model and the geological features of the island was observed, especially in the northern sector where most of the stations are installed. In particular, the top of the high-impedance contrast interface appears deeper in the northern coastal areas and shallower in the central sector. This result agrees with the structural settings of the island likely due to the resurgence of Mount Epomeo.

Key words: Inverse theory; Seismic noise; Volcano seismology; Calderas.

1 INTRODUCTION

Nowadays, a 3-D reconstruction of the deepest parts of volcanic areas from the analysis of seismic ambient noise data by the horizontal-to-vertical spectral ratio (HVSR) technique (Nakamura 1989) is not yet a widely used approach in the scientific community. The effectiveness of evaluating a 3-D model from 1-D inversion models has now been widely demonstrated especially in the sedimentary basin contexts, such as the Pohang basin in South Korea (Kang *et al.* 2020). Additionally, Özalaybey *et al.* (2011) obtained a 3-D model by combining single station microtremor and gravity measurements in the Izmit bay area. Pilz *et al.* (2010) extracted the shear wave velocity structure of the Santiago de Chile basin using 125 single-station acquisitions. Recently, Maghami *et al.* (2021) leveraged the HVSR inversion of microtremor recordings to reconstruct the 3-D shear wave velocity model of deep alluviums of the Qom basin (Iran). To our knowledge, there are no examples of application of such an approach to the Campania region volcanic areas (southern Italy). As it concerns 1-D velocity models, 1-D large scale (up to 2000 m depth) shear wave velocity (*Vs*) profiles of volcanic areas, obtained from joint inversion of both surface wave dispersion and HVSR curves, are available for the Campi Flegrei volcano (Nardone *et al.* 2020a) and the Ischia island (Nardone *et al.* 2020b), both belonging to the Neapolitan volcanic district (southern Italy). In particular, Ischia island (Fig. 1a) is characterized by a complex structural setting due to fault systems and fractures of both tectonic and volcano-tectonic origin (Orsi *et al.* 1991). Currently, the central sector of the island is dominated by a morphological depression ascribed to a caldera that formed about 55 000 yr ago during the Mount Epomeo Green Tuff eruption (Gillot *et al.* 1982). This area, first filled by deposits from the Green Tuff eruption and then by marine deposits, was subsequently affected by considerable resurgence phenomena that induced the fragmentation of the central sector of the caldera into a series of differentially displaced blocks (Fig. 1b). Several authors attribute the resurgence process to a progressive intrusion of a laccolith at shallow depth (Fig. 1c), which would also justify the uplift of the Mount Epomeo block (e.g. Rittman 1930; Sbrana *et al.* 2009; Della Seta *et al.* 2012).

The first seismic models developed for describing the complex geological asset of the Ischia island come from the studies by Strollo

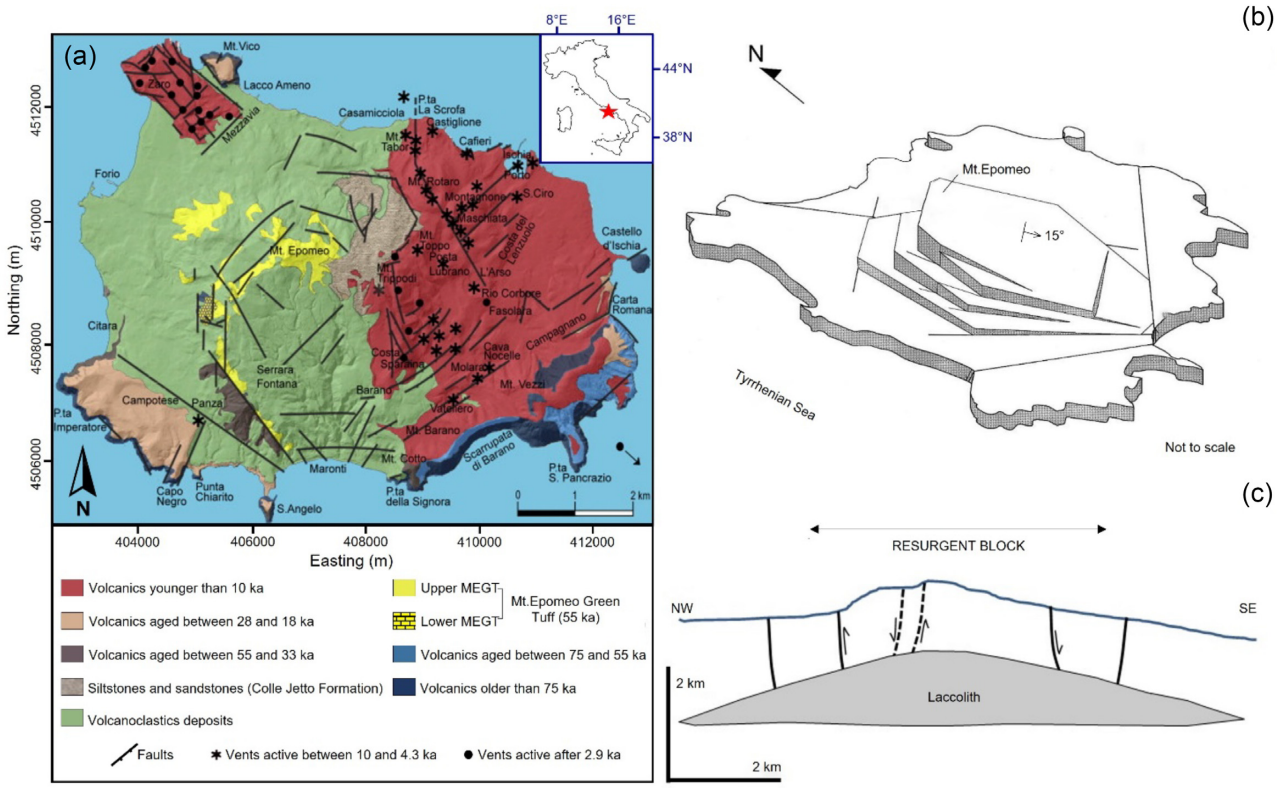

Figure 1. (a) Geological map of the Ischia island (modified from de Vita *et al.* 2006). (b) Fragmentation of the central sector of the caldera into differentially displaced blocks (modified from Acocella & Funiciello 1999). (c) Resurgent block pattern (modified from Nardone *et al.* 2020b).

et al. (2015) and Capuano *et al.* (2015). Strollo *et al.* (2015) by using the frequency time analysis (FTAN) technique, provided 1-D *Vs* velocity models in the first 2 km of depth along 13 paths crossing the island in different directions, while Capuano *et al.* (2015) obtained *P*-wave velocity (*Vp*) models using data from artificial explosions. Conversely, the present work aims to reconstruct a first 3-D *Vs* velocity model of the island from seismic noise records collected at 19 stations belonging to the local monitoring seismic network managed by INGV (Istituto Nazionale di Geofisica e Vulcanologia-Osservatorio Vesuviano, Naples, Italy). The study takes advantage of the preliminary study by Nardone *et al.* (2020b) devoted to the development of a 1-D *Vs* average velocity model of Ischia. From the *Vs* velocity profiles obtained by the inversion of the HVSR curves evaluated for each of the selected seismic stations, a first 3-D *Vs* velocity model of the island is reconstructed to highlight the overall structural characteristics of the volcanic complex.

This paper is structured as follows: at first, a brief outline of advances and limits of the HVSR technique is provided; then, after the presentation of the spectral analysis on broadband noise recordings at 19 sites of the Ischia island, the results of the HVSR curves inversion for each selected site, as well as the final 3-D *Vs* model, are illustrated and discussed in the light of literature stratigraphic and deep well data (e.g. Penta & Conforto 1951; Penta 1963; Agip 1987).

2 METHOD AND DATA

2.1 HVSR technique

Ambient noise-based methods measure a mixture of different waves composing the background noise (Okada 2003) to assess seismic velocity profile of the earth subsurface. Since many sources are located on the earth surface (wind, variation of atmospheric pressure, etc.) or at the bottom of the sea, surface waves dominate the wavefield. One of the most popular methods grounded on ambient noise is the HVSR, because it is a simple way to estimate the dominant frequency induced by local stratigraphy from both microtremor (ambient noise) or earthquake measurements (see Nakamura 1989; Bard 1999). The HVSR technique, originally proposed by Nogoshi & Igarashi (1970), is based on the estimation of the ratio between the Fourier amplitude spectra of the horizontal and vertical components of the ambient noise vibrations recorded at a single seismic station. The method, developed later by Nakamura (1989), is mainly based on two fundamental assumptions: the first one hypothesizes that the soil is composed of a sedimentary layer overlying a rigid half-space; the second hypothesis assumes that the ambient noise vibrations consist mainly of Rayleigh waves. However, with the popularity of the HVSR method application, the precise physical explanation of the results provided by the HVSR technique remains somewhat controversial, mainly related to the nature of the ambient vibration wavefield and its sources. Lunedei & Malischewsky (2015) provided a detailed description of the various theoretical models developed in the last three decades to explain the H/V spectral ratio, identifying two main research lines. One attempts to describe the HVSR curve by taking into account the complete seismic ambient-vibration wave field and the other line just studies the Rayleigh wave ellipticity. After all, many studies have demonstrated that the predominant peak is related to the ellipticity of Rayleigh waves around the site fundamental frequency, f_0, when a significant impedance contrast between the soil and the bedrock is present (Nogoshi & Igarashi 1971; Field & Jacob 1993; Lachet & Bard 1994; Tokimatsu 1995; Konno & Ohmachi 1998;

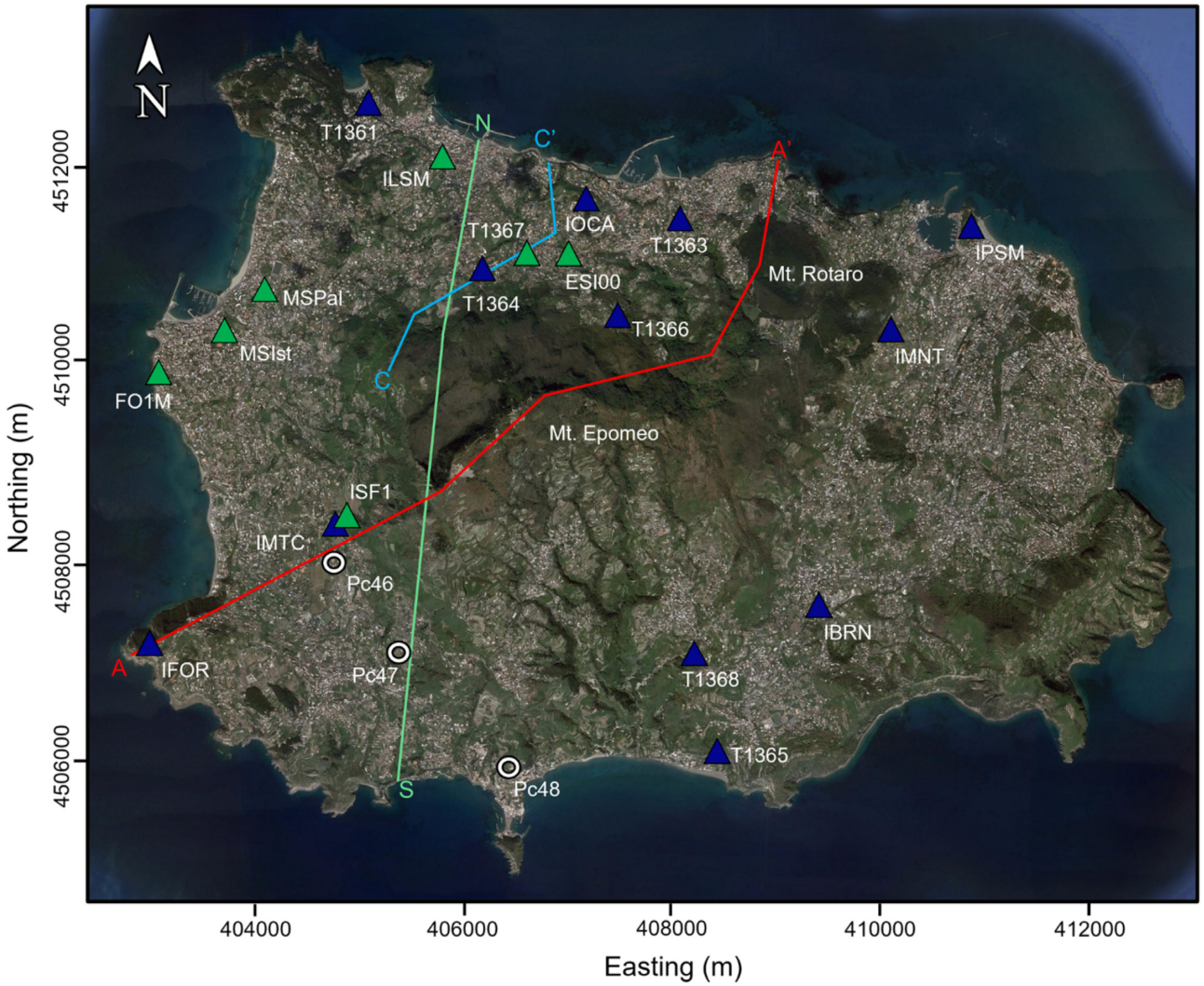

Figure 2. Monitoring seismic network of the Ischia island. The blue triangles show the seismic stations used by Nardone *et al.* (2020b). The green triangles indicate the stations added for the present study. Red, light-blue and green lines delineate the traces of the geological sections used to validate the 3-D *Vs* velocity model. The open white circles show the deep wells located in the southwestern sector of the island.

Table 1. Coordinates of the seismic stations used for the present study. Turquoise background rows indicate the stations shown with green triangles in Fig. 2.

Site Name	Coordinates			Site Name	Coordinates		
	Latitude	Longitude	Elevation (m)		Latitude	Longitude	Elevation (m)
ESI00	40.7434	13.8980	93	**IMTC**	40.7209	13.8758	209
FO1M	40.7334	13.8551	8	**IOCA**	40.7468	13.9014	123
ILSM	40.7508	13.8873	20	**IPSM**	40.7462	13.9439	10
ISF1	40.7210	13.8760	200	**T1361**	40.7567	13.8789	7
MSIst	40.7366	13.8637	16	**T1363**	40.7455	13.9135	50
MSPal	40.7404	13.8670	6	**T1364**	40.7426	13.8905	129
T1367	40.7435	13.8952	81	**T1365**	40.7014	13.9181	130
IBRN	40.7140	13.9268	150	**T1366**	40.7373	13.9046	213
IFOR	40.7115	13.8551	234	**T1368**	40.7108	13.9161	314
IMNT	40.7361	13.9346	180				

Bard 1999). According to Nakamura (1989, 2000), instead, the H/V ratio is related to the transfer function for vertical incidence of horizontally polarized shear (SH) waves. One of the latest interpretations has been proposed by Sánchez-Sesma *et al.* (2011) and Garcia-Jerez *et al.* (2013). They suppose that the microtremors form a diffuse field containing all types of body (*P* and *S*) and surface (Love and Rayleigh) waves. For the first research line, two models of the ambient seismic wave field have been assumed: the distributed

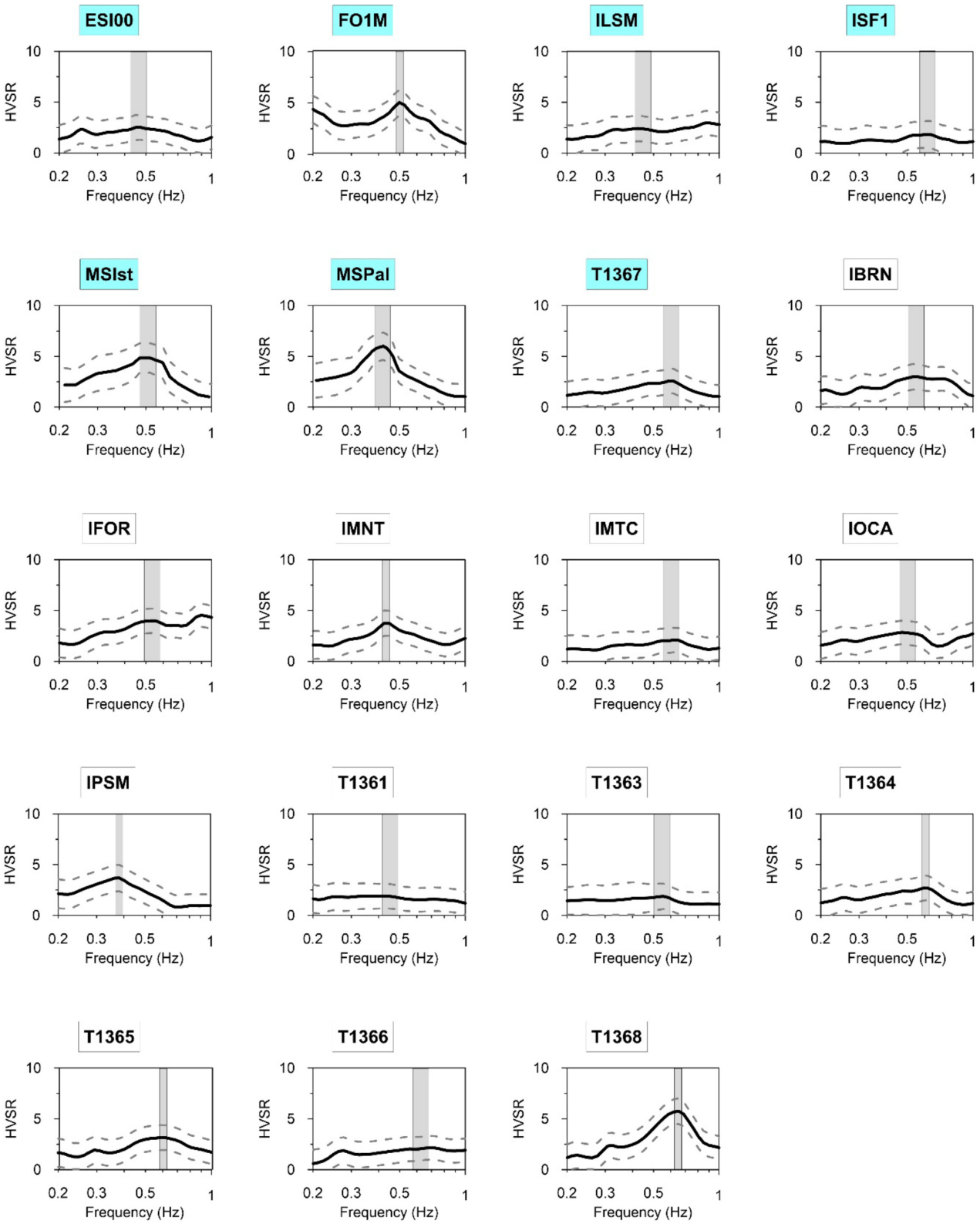

Figure 3. Results of the HVSR analysis. The continuous black curves indicate the HVSR curves obtained from a minimum of 4 hr to a maximum of 24 hr of noise recording; the dashed grey lines indicate the minimum and maximum standard deviation. The grey vertical bands show the fundamental frequency peak with its standard deviation. The turquoise colour identifies the stations added for this study.

surface sources (DSS) model (Albarello & Lunedei 2010; Lunedei & Albarello 2015), and the diffuse field assumption (DFA) model (Sánchez-Sesma *et al.* 2011). García-Jerez *et al.* (2012) compared these two models finding that they provide similar results, particularly with respect to the surface wave behaviour. However, Lunedei & Malischewsky (2015) suggested that further investigations are

Table 2. Input model parameter values used to invert the HVSR curves of each site.

Layer	h (m) min–max	V_p (km s^{-1}) min–max	V_s (km s^{-1}) min–max	ρ (kg m^{-3})	ν min–max
1	80–190	1.1–1.3	0.5–0.6	2000	0.31–0.38
2	175–410	2.2–2.7	1.1–1.3	2200	0.31–0.38
3	390–915	2.8–3.4	1.6–1.9	2400	0.24–0.29
Half-space	-	4.8–5.9	2.7–3.4	2600	0.22–0.27

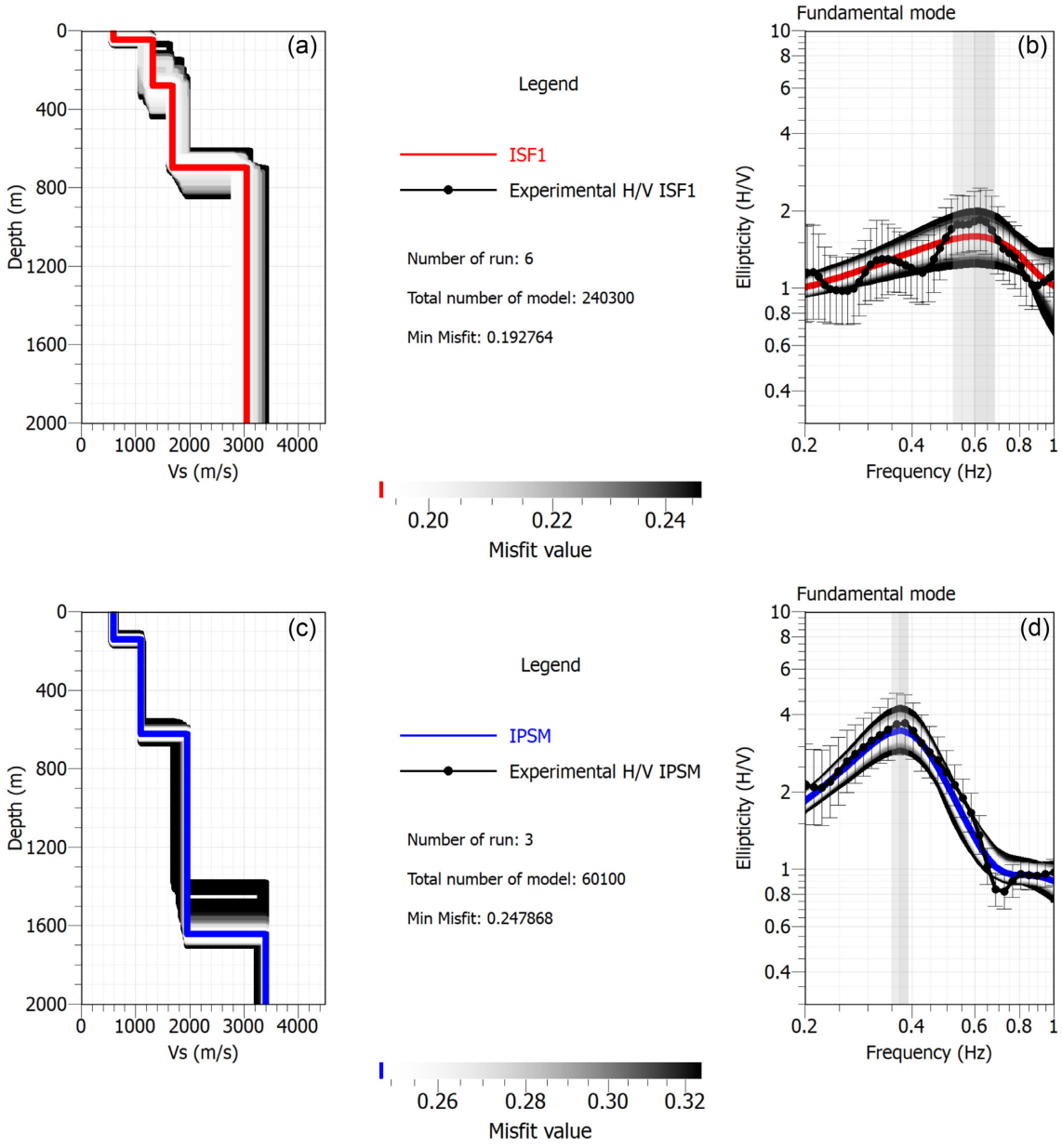

Figure 4. 1-D *Vs* models and ellipticity functions obtained for the station sites ISF1 (a and b, respectively) and IPSM (c and d, respectively). The continuous blue and red lines in (a) and (c) indicate the best solution model for the sites ISF1 and IPSM, respectively; the continuous black dotted lines in (b) and (d) indicate the experimental ellipticity curves for the sites ISF1 and IPSM, respectively, which are compared with the theoretical curves obtained in this study (continuous red and blue lines in c and d).

required to clarify the differences between DFA and DSS models. Regarding the second line of research, in recent years two different techniques have been mainly applied to provide a better estimate of the Rayleigh wave ellipticity: the H/V time–frequency analysis (HVTFA, Poggi & Fäh 2010) and the RayDec method (Hobiger *et al.* 2009). Further studies have shown that, in addition to the good agreement with the HVSR empirical curves and the ellipticity function of the fundamental mode of Rayleigh waves from ambient noise recordings (Lachet & Bard 1994; Fäh *et al.* 2001), the peak frequency is related to thickness and shear wave velocity of

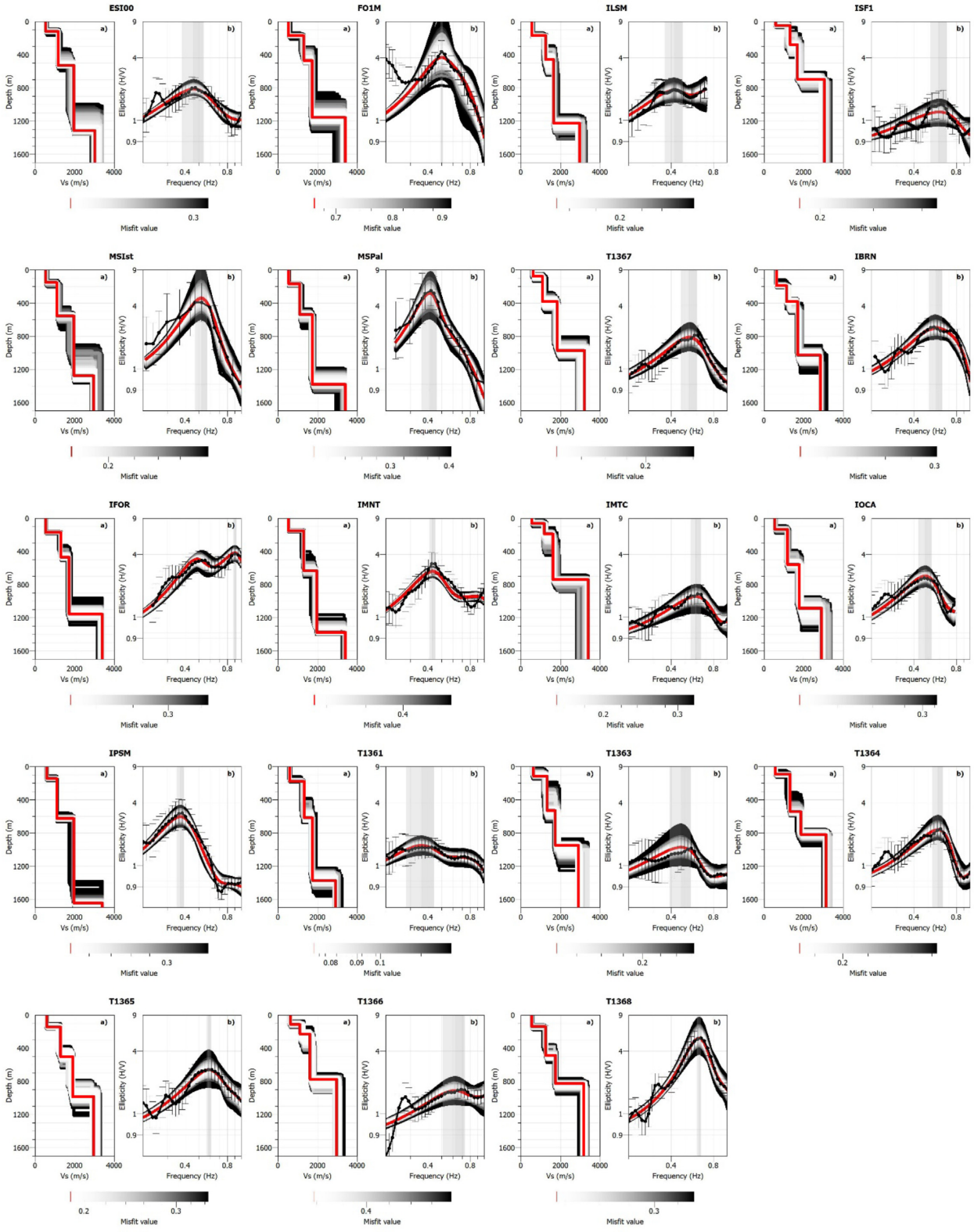

Figure 5. Results of the inversion procedure. For each site, *Vs* model (a), ellipticity function and observed HVSR curve (black dotted lines) (b) are shown. The red lines represent the solutions showing the minimum misfit.

the sedimentary layer. In contrast, the hypothesized proportionality between peak amplitude and impedance contrast between the surface layer and the underlying bedrock is still an open question within the scientific community. Peak's shape depends on the geometry of the subsurface: peaks with narrow bandwidth are mainly associated with strong impedance contrasts, while, in presence of lateral variations in the soil properties (e.g. near valley edges, or in fault areas where lithologically different structures are

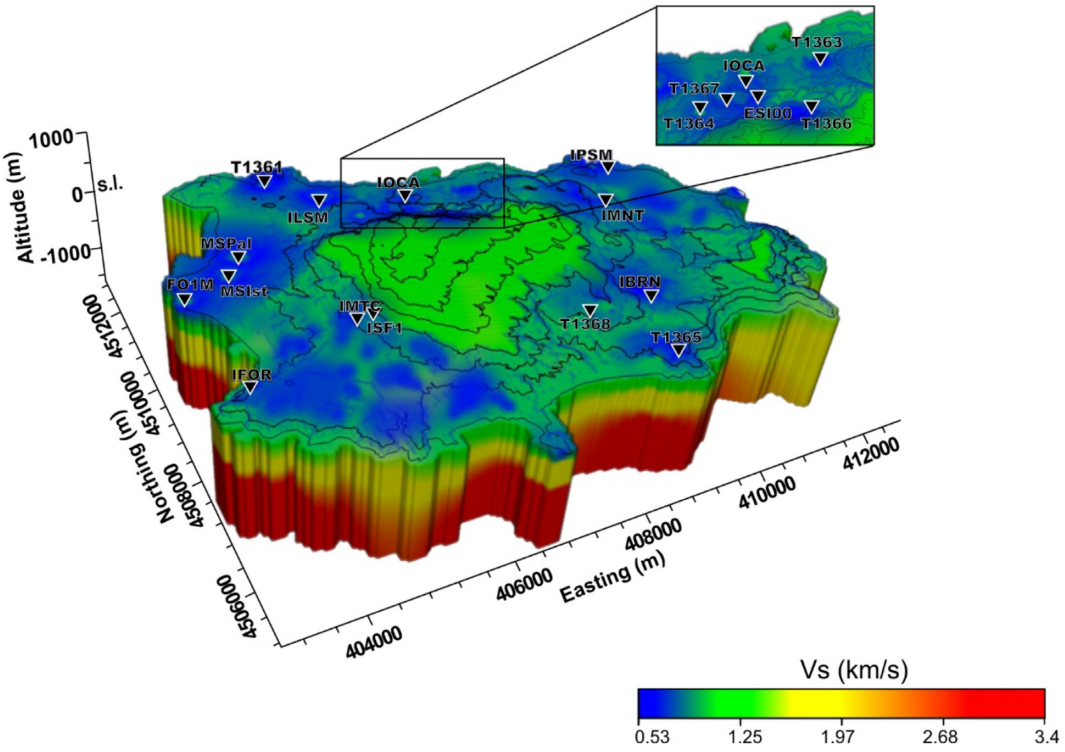

Figure 6. 3-D *Vs* velocity model of the Ischia island. Isolines represent the topography (contour interval is 100 m).

in contact with each other), broad peaks are observed, probably due to a complex wave field that includes diffracted waves from local heterogeneities (Bonnefoy *et al.* 2006). Over time, the HVSR method has been widely applied in various research fields due to its ease of use, despite several weaknesses of the technique that are still a matter of debate (e.g. the understanding of the precise composition of the microtremor wavefield; see Molnar *et al*. 2022 and references therein). In volcanic areas, for example, it is also an effective tool to support the investigation of complex volcanic settings, even where horizontal layering and isotropic site response are not fully verified (Torrese *et al*. 2020). Furthermore, the usage of time-dependent HVSRs has proven to be a useful tool for exploring the shallow velocity structure of a volcanic region (Almendros *et al.* 2004). On the other hand, Panzera *et al.* (2016) tried to infer the depths of the main discontinuities of the subsoil structure in a mud volcanoes area (i.e. Salinelle, Mt Etna, Italy) by combining the HVSR method with the polarization analysis.

It is well known that the HVSR technique is able to assess the resonance frequency of the investigated site, but it is not reliable for the ground motion amplification estimate (Mucciarelli *et al.* 2001). Experimental evidence, indeed, shows that the HVSR allows the retrieval of the fundamental frequency of the sediment but provides an underestimate of the site amplification (Lachet & Bard 1994; Dravinski *et al.* 1996), although, in some cases, the method does not supply an accurate evaluation of both resonant frequency and amplification in the presence of weak impedance contrasts (Luzon *et al.* 2001; Malischewsky & Scherbaum 2004). Furthermore, it is not entirely clear whether this technique can be applied not only to seismic noise but also to earthquakes (Mucciarelli *et al.* 2003). For this purpose, Kawase *et al.* (2011) demonstrated the effectiveness of a new formulation for the average HVSR spectral ratio of earthquake motion. The latter, estimated with an adequately large amount of earthquake data in the Tohoku area (Japan), depends only on the geological structure and not on the data set used to compute it (Ducellier *et al.* 2013). In contrast, the strengths of the methodology are well established in the scientific literature. As well known, the HVSR technique is an approach commonly used to obtain 1-D shear wave velocity models of shallow geological formations. In fact, HVSR curves are also used to estimate depth and thickness of the seismic bedrock, as well as the seismic velocity of the shallower deposits, by 1-D inversion of HVSR curves (Fäh *et al.* 2003; Maresca *et al.* 2012; Martorana *et al.* 2017; Picotti *et al.* 2017). However, the obtained models can have a large margin of uncertainty when the data inversion is not adequately constrained by stratigraphic and/or borehole information, or otherwise (Martorana *et al.* 2018). On more, in some specific applications, HVSR curves jointly with polarization analysis revealed the effect of topography (Napolitano *et al.* 2018). In this work, the inversion results of HVSR curves evaluated for 19 stations belonging to the monitoring seismic network of the Ischia island are analysed and discussed to verify the suitability of the proposed technique in providing a 3-D velocity model of the island characterized by both wide lithological variability and high geothermal gradient.

It is worth to note that, although the morphology of the island is rather complex, especially in the central part that hosts the Mount Epomeo relief, the effects of topographic amplification were considered negligible because the analysed seismic stations are located in hilly areas with slight slope. For our study, velocity values obtained by Nardone *et al.* (2020b) were used as a constraint in the inversion procedure applied to each site.

2.2 Data set

Ambient seismic noise signals used in this study have been recorded by the digital three component seismic stations of the monitoring

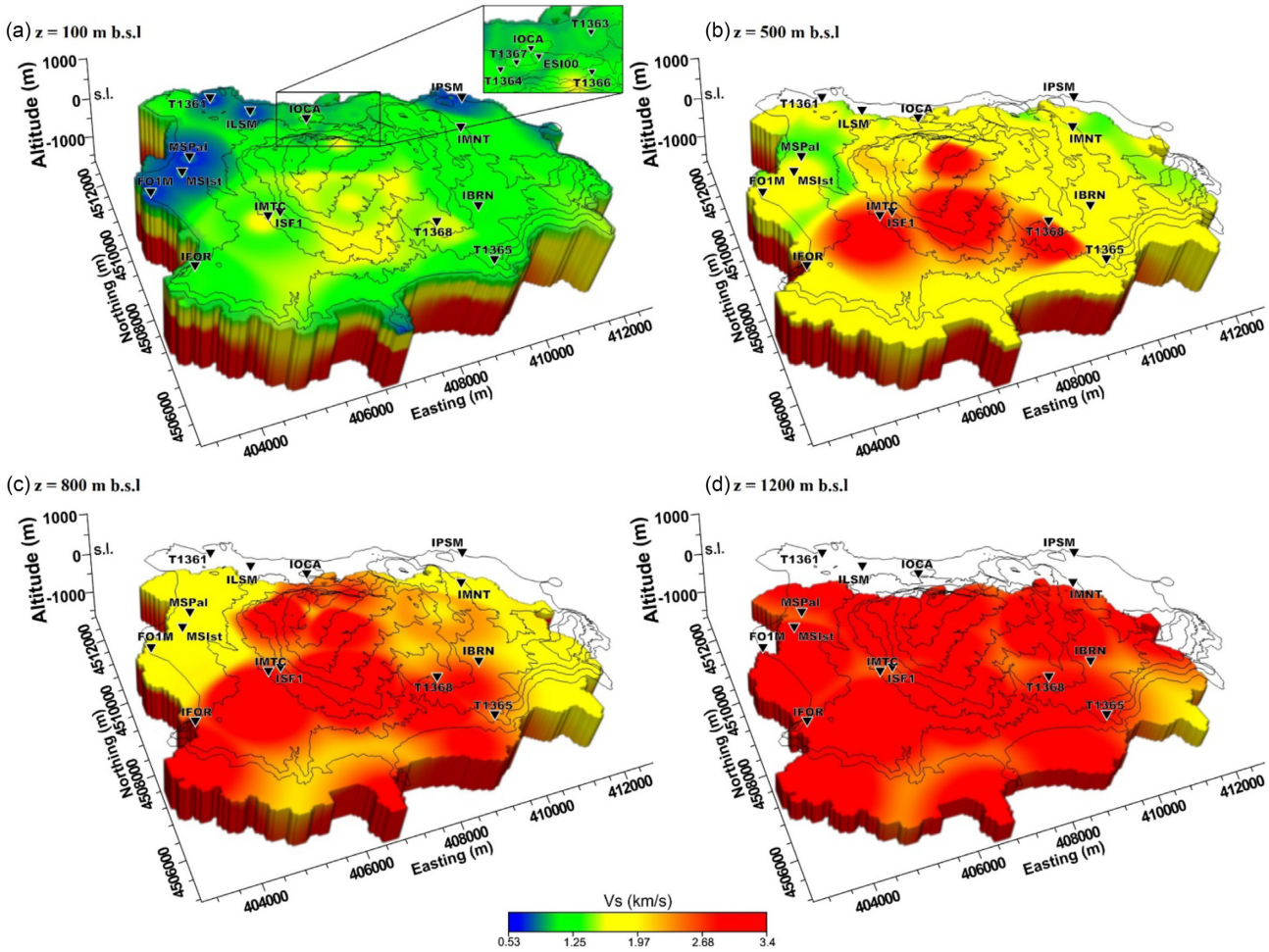

Figure 7. Horizontal cuts of the 3-D *Vs* velocity model at four different depths below sea level (b.s.l.). Isolines represent the topography (contour interval is 100 m).

network at Ischia operated by INGV and recently improved (Fig. 2). In fact, following the M_w 3.9 earthquake occurred on 21 August 2017, some mobile seismic stations were added to the permanent network (Galluzzo *et al.* 2019) and acquired data for about three years (Galluzzo *et al.* 2017). In particular, the dataset used for our study consists of seismic noise recorded at 19 station sites (Table 1) during the time interval ranging from 2018 to 2021. Compared to the seismic stations used by Nardone *et al.* (2020b), other seven stations have been added (turquoise rows in Table 1). They are mainly located in the western sector of the island (Fig. 2), where initially a low number of station sites was available. The improvement of the seismic network has allowed a wider azimuthal coverage for the reconstruction of the main underground physical/structural discontinuities. Seventeen out of nineteen sites are equipped with broadband sensors (Lennartz LE3D20s and Guralp CMG 40T) and have been installed and managed by INGV (Orazi *et al.* 2018; Galluzzo *et al.* 2019). Some of these stations record at 125 sample per second (sps), others at 100 sps. The remaining two sites (MSPal and MSIst), situated in the NW sector of the island (Fig. 1), represent the locations of some HVSR passive single-station surveys ('Geobox' triaxial seismograph by Sara Instruments) carried out in the framework of the 3rd level seismic microzonation in the Municipality of Forio (http://www.commissarioricostruzioneischia.it/Esiti-Microzonazione.html).

3 RESULTS

3.1 HVSR analysis

Starting from the results by Nardone *et al.* (2020b) and taking into account the significant geological-structural characteristics of the Ischia island, as well as the mutual distances between the stations, we focused our spectral analysis in the frequency band 0.2–1 Hz. In particular, the mean velocity model obtained from the joint inversion of the HVSR and surface wave dispersion curves reported in the above-mentioned study was used as starting model for the inversion process, which was carried out by assuming that the HVSR curve of each site is theoretically related to the Rayleigh wave ellipticity of the fundamental mode (Fäh *et al.* 2001; Lunedei & Albarello 2010; Foti *et al.* 2018). Spectral ratios of seismic noise recorded at the 19 stations sites in Table 1 were calculated using the GEOPSY package (Wathelet *et al.* 2004, 2020). The analysis was performed by using 120 s sliding time windows with a 5 per cent overlap; selected signals were at first tapered by cosine function, and the amplitude spectra were smoothed by the Konno and Ohmachi method (Konno & Ohmachi 1998). In addition, as a first step in the followed procedure, the removal of spikes due to phenomena of non-natural origin, such as instrumental and/or artificial noise, was performed.

The results of the HVSR analysis are shown in Fig. 3, where the continuous black curves indicate the HVSR curves obtained from

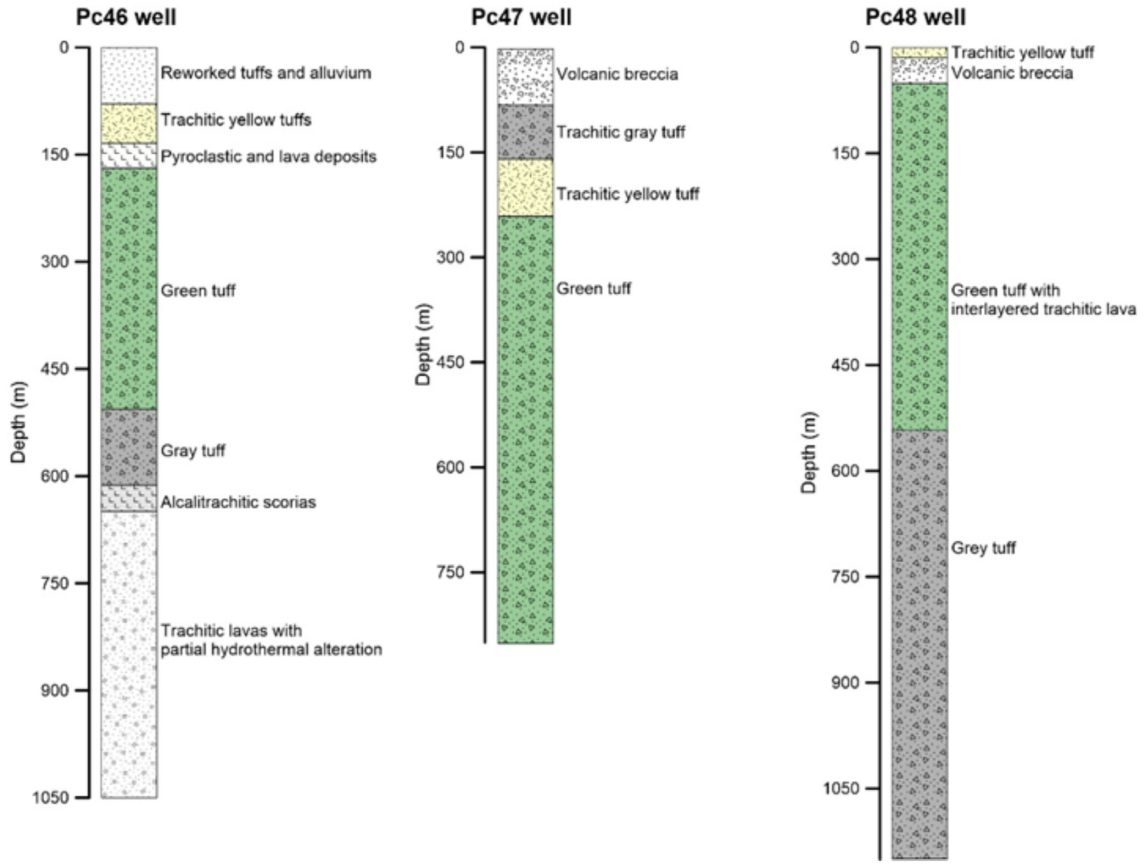

Figure 8. Stratigraphy of the deep wells Pc46, Pc47 and Pc48 shown in Fig. 2 with open white circles (modified from Carlino *et al.* 2014).

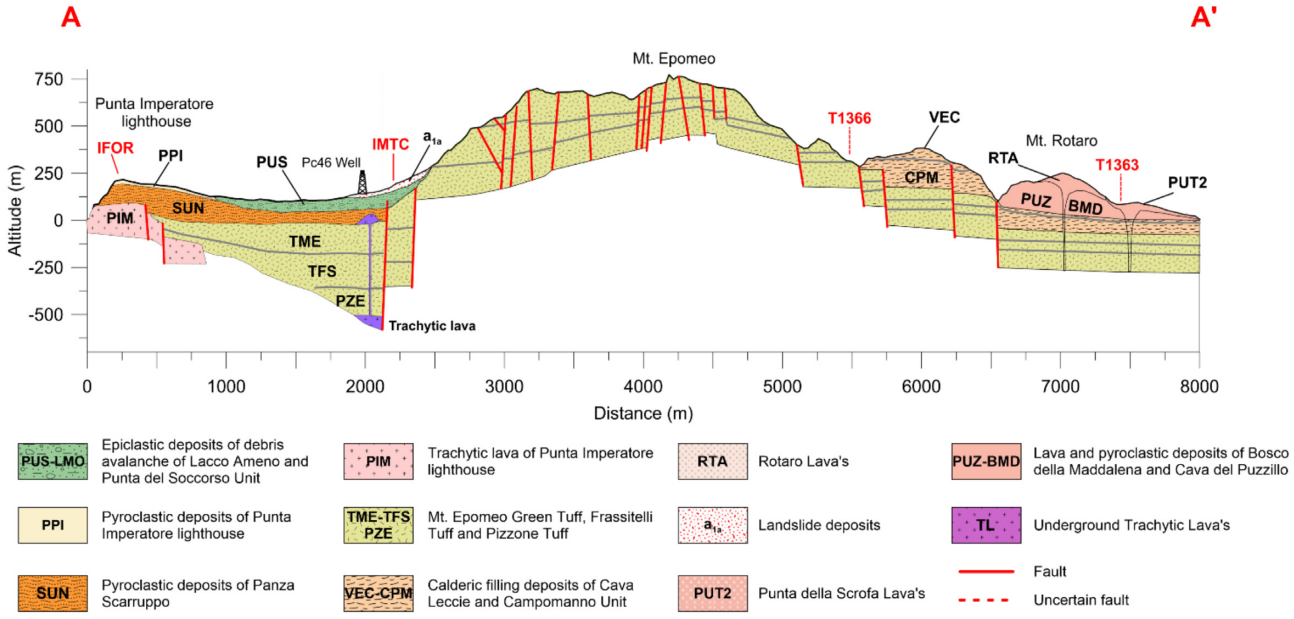

Figure 9. CARG AA' section (modified from Sbrana & Toccaceli 2011).

a minimum of 4 hr to a maximum of 24 hr of noise recording. The selection was done by visual inspection excluding signals containing local disturbances and lack of data due to the records transmission. The grey vertical bands show the fundamental peak frequency with its standard deviation. Spectral ratios for frequencies greater than 1 Hz were excluded from the analysis because their shapes showed significant differences most likely related to very local geological-structural conditions of the site, which were not taken into account in this work. As shown in Fig. 3, the frequency peaks for the new sites (i.e. ESI00, ISF1, T1367, FO1M, MSPal, MSIst and ILSM) are observed below 0.8 Hz. The obtained results agree with those shown in Nardone *et al.* (2020b): moving from the centre of the

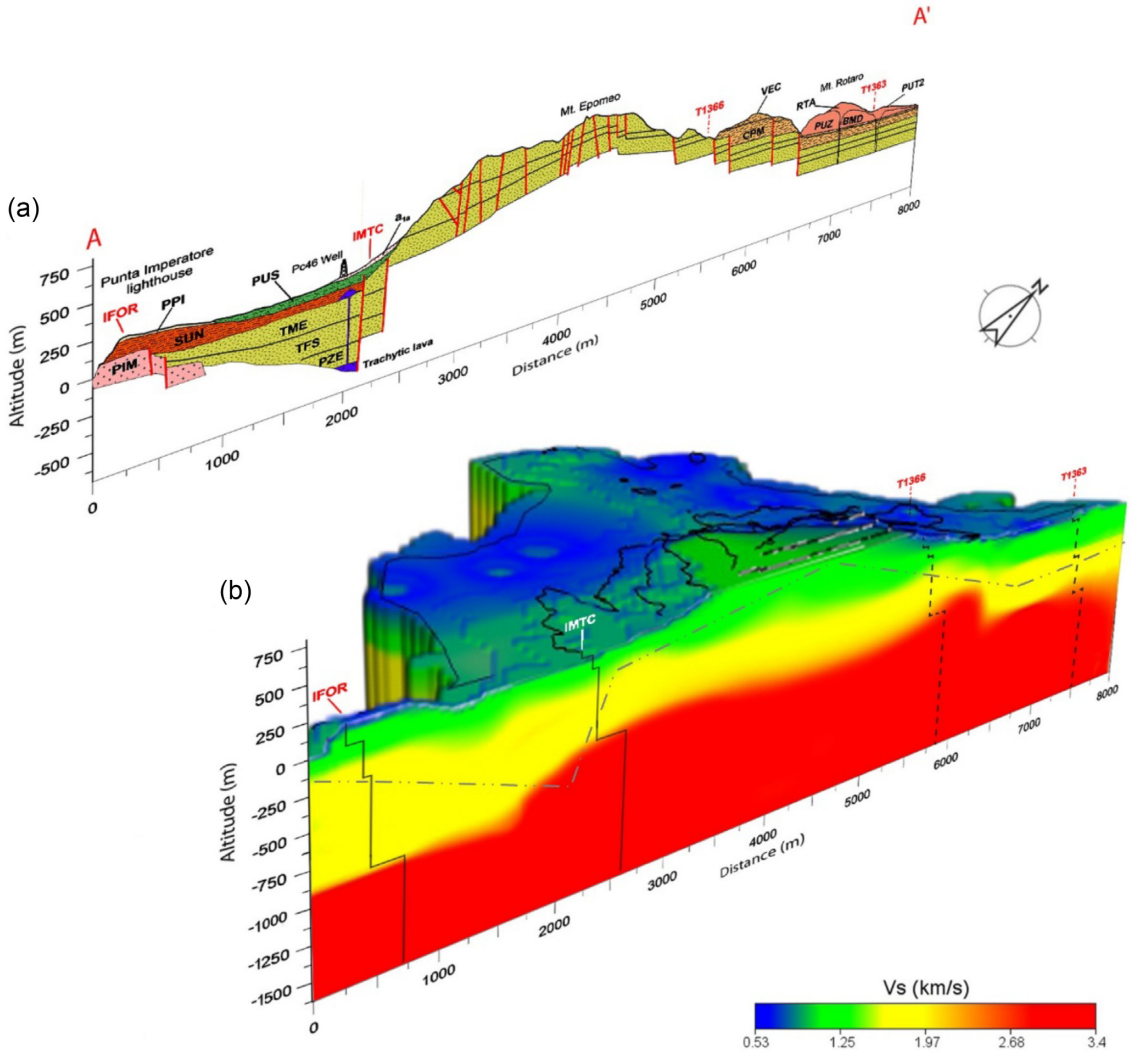

Figure 10. (a) CARG AA' Section (modified from Sbrana & Toccaceli 2011). (b) Clip plane of the 3-D *Vs* model in Fig. 6 along a direction approximately coincident with the AA' section. The *Vs* profiles related to the intercepted seismic stations are also indicated. The continuous black lines show the profiles that fall exactly along the section, while the dashed black lines mark the projections of the profiles located about 1 km west of the section. The grey dashed line sketches the in-depth geometry of the corresponding CARG AA' section.

island towards the coast, the frequency peaks move towards the low frequencies (from 0.6 Hz for T1366 to 0.37 Hz for IPSM).

3.2 Data inversion

The inversion procedure adopted to obtain the 1-D velocity models for the 19 analysed sites is based on the Neighbourhood Algorithm implemented in the DINVER tool of the GEOPSY package (Wathelet *et al.* 2008). The algorithm provides the best velocity model by performing a stochastic search in a multiparameter space to identify the impedance surface and its variations. The calculated parameters, that is thickness, *P*-wave velocity, *S*-wave velocity, density and Poisson's ratio (here after identified as h, Vp, Vs, ρ and ν, respectively), define a sequence of n layers that overlay the half-space. In particular, we assumed that the *S*-wave velocity varies in a very small range (tolerance of 10 per cent) according to the 1-D model in Nardone *et al.* (2020b) and modified the layer thicknesses to obtain the corresponding 1-D *Vs* models. This is reasonable as the Rayleigh wave velocities depend strongly on the *Vs* structure and weakly on the other parameters (Wathelet *et al.* 2005). To constrain the peak of the HVSR curves (which holds significant information about the depth of the bedrock), we considered both left and right limb of the HVSR curve as well for the inversion, therefore the frequency range of the HVSR spans from 0.2 to 1 Hz. According to the large-scale 1-D model obtained by Nardone *et al.* (2020b), we used the starting model parameters shown in Table 2, where the layer densities are the same reported in Nardone *et al.* (2020b), while the velocities are set to vary by 10 per cent with respect to the average velocity value of the 1-D model. Finally, the variation range of the layer thicknesses is fixed at 40 per cent. These settings (wave velocity and thicknesses range) were chosen on the basis of the morpho-stratigraphic features of the deeper layers found in literature (Acocella & Funiciello 1999). We note that the model parameters in Table 2 represent the best-fit solutions of the parametric study reported in Nardone *et al.* (2020b). These authors, in fact, extensively explored the influence of the initial velocity values on the inversion process through a join inversion of the Rayleigh wave dispersion curve and the mean HVSR. This approach significantly reduces the problems connected with non-uniqueness of the solution when the single HVSR inversion is used.

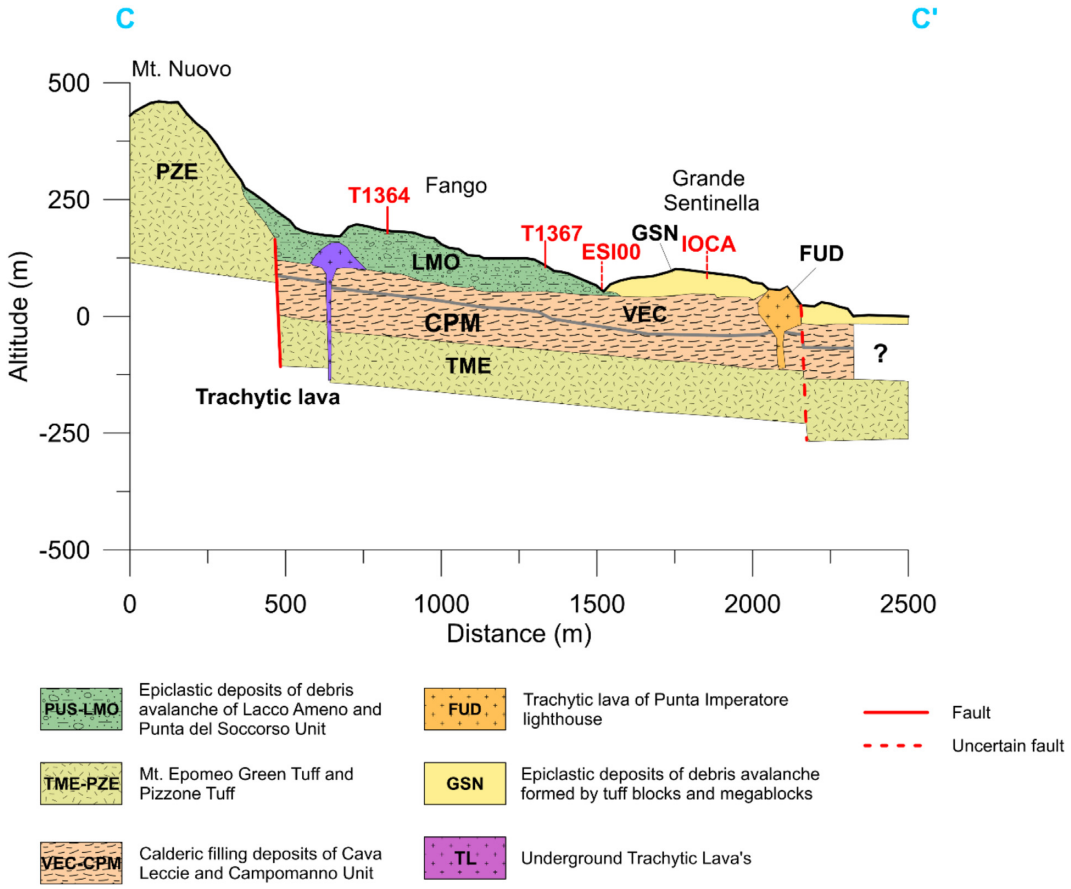

Figure 11. CARG CC' section (modified from Sbrana & Toccaceli 2011).

The best-fitting curve for each site was obtained for no more than 13 iterations (the maximum number of iterations was reached for the IOCA station). For all the sites, the models that show the best fit solution consist of subsoils composed of three main seismic layers, characterized by *Vs* velocities increasing with depth, which are laid on a half-space. For the sake of brevity, we describe in detail only the inversion results obtained for the sites ISF1 and IPSM (Fig. 4), which identified the most representative areas of the island, that is those defined by the minimum and maximum depth value of the deepest layer, respectively. The ISF1 *Vs* profile (continuous red line in Fig. 4a), characterized by three layers lying on a half-space at a depth of 700 m below ground level (b.g.l), is the result of a stochastic search among more than 240 000 possible models (minimum misfit equal to 0.19). As regards the ellipticity, an acceptable fit between theoretical and experimental curves is found (Fig. 4b). For the IPSM site, the best solution model (continuous blue line in Fig. 4c), obtained by an inversion process that investigated more than 60 000 possible models in the parameter space (minimum misfit equal to 0.24), is described by three seismic layers lying on a half-space at a depth of about 1600 m b.g.l. In addition, an excellent match between theoretical and experimental ellipticity curves is observed (Fig. 4d). However, we note that the HVSR inversion curves related to the whole set of analysed station sites (Fig. 5) identify the top of the half-space at shallower depths in the central-southern sector of the island (e.g. ISF1, IMTC, T1366 in Fig. 2, with higher HVSR frequency peaks), while it is found deeper in the northern sector (e.g. IPSM, FO1M in Fig. 2, with lower HVSR frequency peaks). As it can be seen in Fig. 5, the *Vs* models and ellipticity curves are shown, respectively, to the left and to the right of each plot. The best-fitting models (red curves) obtained for all the sites show low misfit values indicating a good convergence in the space of the parameters. Generally, for the sites located along the coast of the island, the top of the half-space appears deeper than that identified by the sites located in the central part of the island, due to the rise of Mt Epomeo (Orsi *et al.* 1991).

3.3 A first 3-D *Vs* model of the Ischia island

The 1-D models obtained for the analysed seismic stations were used for reconstructing the first 3-D *Vs* model of the Ischia island shown in Fig. 6. It was achieved by interpolating over a grid with a spacing of 65, 50 and 40 m in the easting, northing and elevation directions, respectively. We are aware that the retrieved 3-D model is based on a number of stations that are quite scattered, especially for the central and eastern sectors, and not sufficient for a detailed reconstruction of the whole island. However, it can be considered reliable mostly for the northern and western parts of the island, where a greater number of seismic stations are available and a good agreement is observed with the results of previous geological and geophysical studies, as it will be seen in the next section.

The 3-D *Vs* model in Fig. 6 shows a sequence of 4 seismic layers characterized by the following velocity ranges:

1st layer (blue shades): 0.53–0.63 km s^{-1}

2nd layer (green shades): 1.09–1.32 km s^{-1}

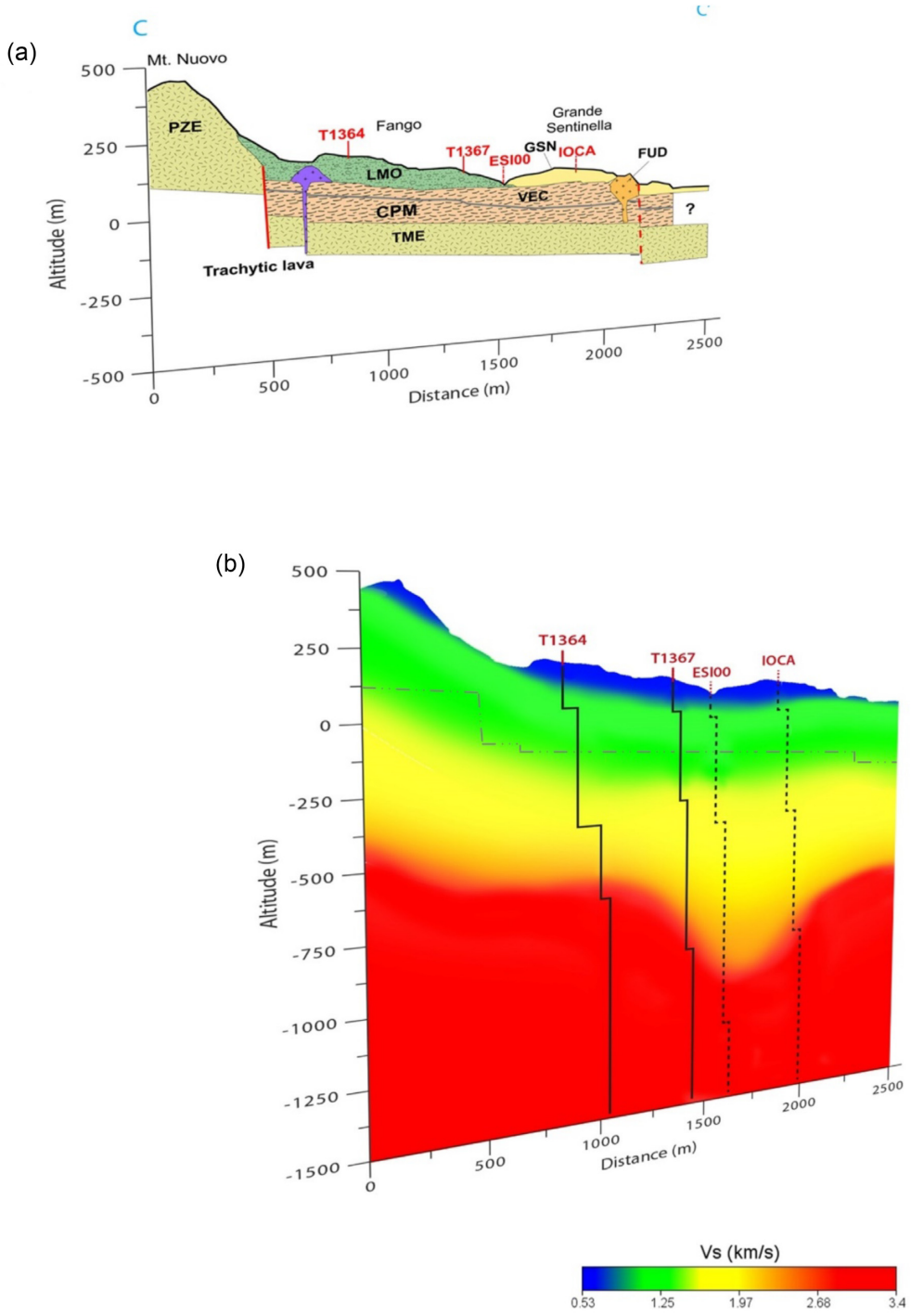

Figure 12. (a) CARG CC' section (modified from Sbrana & Toccaceli 2011). (b) Clip plane of the 3-D *Vs* model in Fig. 6 along a direction approximately coincident with the CC' section. The *Vs* profiles related to the intercepted seismic stations are also indicated. The continuous black lines show the profiles that fall exactly along the section, while the dashed black lines mark the projections of the profiles located about 200 m east of the section. The grey dashed line sketches the in-depth geometry of the corresponding CARG CC' section.

3rd layer (yellow shades): 1.61–1.95 km s^{-1}

4th layer (red shades): 2.87–3.40 km s^{-1}.

Fig 7, which highlights the *Vs* discontinuity surfaces for increasing depths, shows the top of the deepest layer, characterized by the highest *Vs* values observed for the stratigraphic sequence, at a depth of about 500 m b.s.l. in the central part of the island (Fig. 7b) that extends at greater depths to cover the whole island (Figs 7c and d).

4 VALIDATION OF THE 3-D *Vs* MODEL

To verify the reliability of our study, we compared the obtained 3-D *Vs* model of Ischia with the results of previous geological and geophysical studies. Specifically, we considered two geological sections, AA' and CC' in Fig. 2, realized in the framework of the Geological CARtography (CARG) Italian project (Sbrana & Toccaceli 2011), and a N–S magnetotelluric profile (green line in Fig. 2)

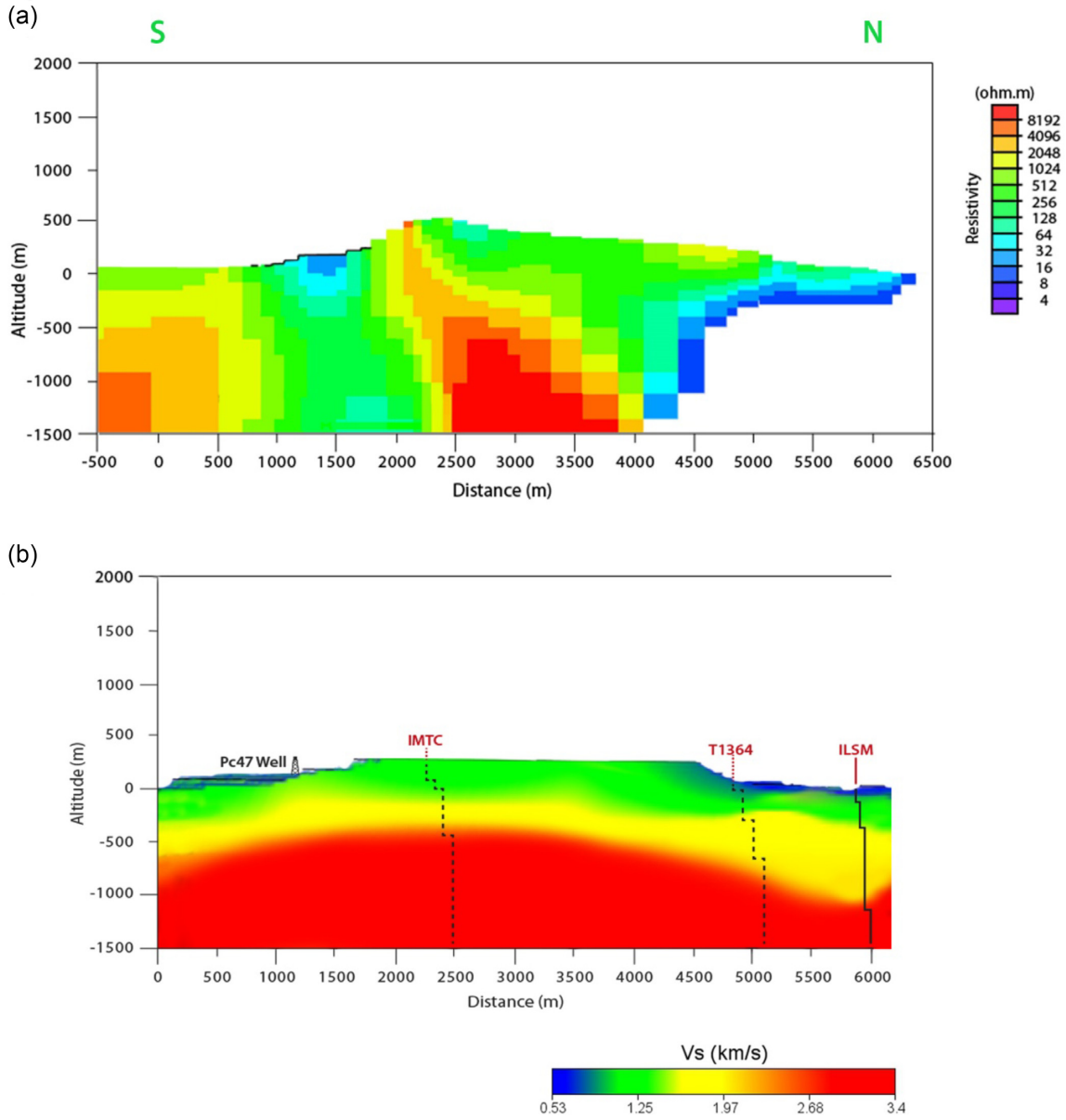

Figure 13. (a) N–S resistivity section retrieved by magnetotelluric soundings (modified from Di Giuseppe *et al.* 2017). (b) Clip plane of the 3-D *Vs* model in Fig. 6 along a direction approximately coincident with the N–S section. The *Vs* profiles related to the intercepted seismic stations are also indicated. The continuous black lines show the profiles that fall exactly along the section, while the dashed black lines mark the projections of the profiles located about 500 m west of the section.

carried out by Di Giuseppe *et al.* (2017). In addition, stratigraphic logs (Fig. 8) from deep wells (open white circles in Fig. 2, Penta & Conforto 1951; Penta 1963; Agip 1987) were also taken into account.

The SW–NE CARG section (AA' in Fig. 9) crosses the Mt Epomeo resurgent block and intercepts the seismic stations IFOR and IMTC in its southernmost part, while it is about 1 km west from the T1366 and T1363 stations located in the northern portion of the Island (see Fig. 2). Comparing the CARG AA' section with the 3-D *Vs* model, suitably cut along a direction coinciding approximately with the direction of the AA' section (Fig. 10b), clear correlations emerge between the geological and velocity models, which are also supported by the stratigraphy of the deep well Pc46 (Fig. 8). For a more straightforward interpretation of the correspondences between the two models, the 1-D velocity profiles for the seismic stations located along or near the AA' profile are also plotted in Fig. 10(b). The *Vs* profile corresponding to the IFOR site shows a first seismic layer defined by thickness (∼150 m) and velocity (∼500 m s^{-1}) values that well correlate with the pyroclastic deposits of Punta Imperatore lighthouse (PPI, thickness ∼30 m) and Panza Scarrupo (SUN, thickness ∼120 m) (Fig. 10a), the latter constituted of different types of weakly cemented pyroclastites formed by medium and thin layers of lapilli and pumiceous bombs (see Fig. 9). Thickness and velocity of the second layer, respectively ∼300 m and ∼1300 m s^{-1}, can be linked to the Punta Imperatore lavas (PIM deposit in Fig. 10a), that is compact and massive scoriaceous lavas of trachytic composition (see Fig. 9). Although the CARG section does not provide information for depths greater than a few tens of metres below sea level, the *Vs* model clearly identifies a discontinuity surface that could correspond to the top of the laccolith at a depth

of ∼1200 m b.g.l (top of the red layer in Fig. 10b). The velocity profile for the IMTC site agrees well with the stratigraphy of the adjacent Pc46 well (see Fig. 2), which reaches a maximum depth of 1050 m b.g.l. (Fig. 8) and the AA' geological section (Fig. 9). The first seismic layer, in fact, with thickness of ∼60 m and velocity of ∼550 m s^{-1}, can be associated to the reworked tuffs and alluvium deposits provided by the Pc46 stratigraphic log (a1a deposit in Fig. 9), while the second seismic layer (thickness of ∼130 m and velocity of ∼1200 m s^{-1}) seems to describe well the Punta del Soccorso Unit (PUS deposit in Fig. 10a), that is epiclastic deposits of debris avalanche formed by tuff blocks and megablocks (see Fig. 9). The third seismic layer, characterized by thickness of ∼500 m and velocity of ∼1600 m s^{-1}, correlates well with the sequence of tuffs shown in the Pc46 stratigraphic column (Fig. 8), corresponding to the Mt Epomeo Green tuff, Frassitelli tuff and Pizzone tuff (TME, TFS and PZE deposits, respectively, in Fig. 9). The fourth seismic layer, identified at a depth of ∼750 m b.g.l, shows very high velocity values (∼3400 m s^{-1}) likely correlated with the trachytic lava deposit identified in the stratigraphic sequence of the Pc46 well (Fig. 8). We attribute the top of this fourth layer to the summit part of the laccolith that, in this sector of the island, would rise by virtue of the Mt Epomeo resurgence. Finally, as it concerns the northern part of the 3-D *Vs* model, we tentatively correlate the T1366 and T1363 velocity profiles with the northern portion of the CARG AA' section, although the two seismic stations do not exactly fall along it. T1366 velocity model is characterized by a first layer defined by thickness of ∼ 120 m and seismic velocity of ∼600 m s^{-1} that is ascribable to altered Green Tuff deposits of the Mt Epomeo eruption (TME in Fig. 9). As for the IFOR site, there are no stratigraphic information for greater depths (see Fig. 9); therefore, thickness (∼110 m) and velocity (∼1100 km s^{-1}) of the second layer individuated by the velocity profile (Fig. 10b) can be linked to the TFS and PZE formations constituted of massive deposits of strongly welded tuffs (Sbrana & Toccaceli 2011). Whereas it is reasonable to attribute the last velocity discontinuity identified at depth of ∼800 m b.g.l. to the laccolith top (Fig. 10b). Finally, as for the T1363 model, a correlation with the AA' section is possible only for the second seismic layer that, based on the observed thickness (∼400 m) and velocity (∼1300 m s^{-1}) values, can be associated to the TFS and TME formations (Fig. 9). Furthermore, the high velocity contrast highlighted at the depth of ∼950 m b.g.l could indicate, according to the other analysed 1-D models, the deepening of the laccolithic structure in the northern sector of the island (Fig. 10b). Considering that the T1363 profile is far from the CARG AA' section about 1 km, we are not confident in assuming a link between the first seismic layer of the profile and the shallowest portion of the section (Fig. 9). In fact, the parameters that characterize a such layer (thickness ∼110 m and velocity ∼630 m s^{-1}) can be consistent both with the RTA and PUZ-BMD lavas (Fig. 9), observed along the northernmost part of the section, and with the tuffs covered by clays of marine origin derived from the calderic filling process (VEC and CPM units in Fig. 9), which more properly describe the shallow deposits of the area where the measurement stations are located.

Fig. 11 shows the CARG CC' section (Sbrana & Toccaceli 2011) sited in the northwestern sector of the Ischia island (see Fig. 2), which intercepts the seismic stations T1364, T1367, ESI00 and IOCA. The corresponding velocity section (Fig. 12b), obtained by cutting the 3-D velocity model along a direction approximately coincident with the CARG CC' profile, show a layers' sequence whose characteristic parameters agree with the geostratigraphic sequence shown in the CC' section. Indeed, thickness and velocity values of the first three seismic layers well describe the geological formations presented in the CARG section, which are constituted of landslide and backfill deposits (PUS-LMO and VEC-CPM in Fig. 11), and different tuff formations (PZE-TME in Fig. 11). Differently from the velocity section correlated with the CARG AA' section (see Fig. 10b), which delineate a layers' morphology relatively homogeneous, the pattern of the second and third discontinuity observed in the velocity model of Fig. 12(b) is more complex, probably due to local structural heterogeneities. It is worth noticing that the third discontinuity, which we attribute to the top of the laccolithic formation, is identified at depths comparable with those retrieved for the seismic section along the AA' profile (Fig. 10b).

Finally, Fig. 13 compares the N–S magnetotelluric (MT) section (Fig. 13a) by Di Giuseppe *et al.* (2017) with the proposed 3-D *Vs* model in Fig. 6, which is cut along a direction roughly coinciding with the MT profile (Fig. 13b). To better interpret the possible correlations between the resistivity and velocity models, the 1-D velocity profiles for the seismic stations located approximately along or in proximity to the MT profile (i.e. ILSM, T1364 and IMTC) are also shown in Fig. 13(b). The latter highlights a very good agreement with the central part of the resistivity section (Fig. 13a), which shows a very resistive block (resistivities >4000 Ωm) compatible with the characteristic parameters (depth and velocity) of the fourth seismic layer (see Fig. 13b). This resistive structure, attributed by Di Giuseppe *et al.* (2017) to crystalline rocks, supports again the laccolith intrusion hypothesis. The lack of MT data in the northernmost part of the section (Fig. 13a) does not allow to compare the morphology of such high-resistivity body with the corresponding high-velocity structure (Fig. 13b). In this sector of the island, in fact, a possible comparison is allowed only for the shallowest seismic layers (see ILSM and T1364 profiles in Fig. 13b), whose depths are fully consistent with those of the electro-layers identified by the MT prospecting (Fig. 13a). Regarding the southern part of the MT section, we do not consider appropriate to compare it with our velocity model because of the inhomogeneous distribution and the low number of seismic stations in this portion of the island. However, we underline the good correspondence between the stratigraphy of the Pc47 well (Fig. 8) and the velocity layers highlighted by the *Vs* model in terms of both depth and geological characteristics. Specifically, we refer to the velocity contrast observed at the depth of about 250 m b.g.l (Fig. 13b) that likely separates the trachytic formations of gray and yellow tuff from the thick deposit of green tuff. The latter, indeed, would be associated with higher velocity values than those the overlying tuff formations because of a denser matrix (Villaseñor 2010).

It is worth noting that, due to the resolution of the proposed *Vs* model, we do not consider it appropriate to validate the results observed in the eastern sector of the island with previous literature studies. The latter, in fact, generally refer to analyses of very shallow deposits attributable to the recent volcanic activity of Ischia (e.g. Sbrana *et al.* 2018).

5 CONCLUSIONS

The 3-D shear wave velocity model obtained for the Ischia island well compares with geological and geophysical literature data, thus supporting the reliability of our approach, based on HVSR inversion and, mainly, its versatility in the use of non-synchronous seismic records. In particular, the proposed model allowed us to correlate the deepest velocity discontinuity to the emplacement of the crystallized laccolith hypothesized by several authors (e.g. Paoletti *et al.* 2009; Sbrana *et al.* 2009; Carlino 2012; Capuano *et al.* 2015;

Strollo *et al.* 2015). The top of the laccolith intrusion (shear wave velocity greater than 3 km s^{-1}) has been identified between ∼500 m and 600 m b.s.l. in the central part of the island, while it deepens up to 1200–1600 m b.s.l. in the northern coastal area. This finding also agrees with the magnetotelluric observations by Di Giuseppe *et al.* (2017). On the contrary, some works (e.g. Paoletti *et al.* 2017) identified the top of the trachytic basement at depths shallower than those observed by our study. This apparent discrepancy is probably due to the high degree of hydrothermalization and fracturing of the uppermost part of the laccolytic intrusion as assumed by the same authors. Furthermore, the *Vs* values retrieved for the shallow deposits (in sequence: alluvium, pyroclastites, green and grey tuff deposits), which range between ∼0.5 and 2.0 km s^{-1}, are consistent with density values found for the investigated area (Berrino *et al.* 2008). The obtained 3-D velocity model, although reconstructed using a non-homogeneous distribution of the seismic station sites, is a first step towards a 3-D image of the *S*-wave velocity distribution for the Ischia island that was not available before. Indeed, some velocity models are found in the literature (Capuano at al. 2015; Strollo *et al.* 2015) obtained with different typologies of seismic signals (seismic noise, artificial shots) and experimental setup (low number of seismic stations). The novelty of the proposed 3-D velocity model with respect to the previous ones consists of a larger areal coverage and number of seismic stations, and of broad band noise recording, which allowed to manage high quality data to investigate larger wavelength and deep structures. In fact, several hours of high-resolution seismic noise acquisition at frequencies lower than 1 Hz allowed us to obtain robust results and to adopt inversion algorithms to obtain reliable *Vs* estimates down to more than 1 km depth. It is worth noticing that our velocity model provides thicknesses and velocities comparable with those obtained by Strollo *et al.* (2015). On the contrary, greater differences are observed with respect to the velocity model proposed by Capuano *et al.* (2015), which is based on the estimate of *Vp* values. Indeed, by deriving the *Vs* values from a *Vp*/*Vs* ratio = 1.88, we observe that their model is slower and consists of two seismic layers on a half-space. These discrepancies are probably due to a different resolution resulting from the number of seismic stations, the azimuthal coverage and the type of dataset derived from artificial shots. As previously highlighted, we are aware of the strong limitations of our result due to both non-homogeneous distribution of stations and small number of measurement points. Notwithstanding, in the sectors uncovered by the seismic network, our results agree with those from other types of data. In particular, for the south-western area, the magnetotelluric profile by Di Giuseppe *et al.* (2017) and the stratigraphy of wells support our findings. Furthermore, the *Vs* velocity model by Strollo *et al.* (2015) in correspondence of the Mt Epomeo perfectly matches our model in terms of both depth and velocity. Despite these critical issues, we believe that the improvement of the velocity model for a heterogeneous medium, such as that of the volcanic island of Ischia, represents an important step for understanding its internal dynamics as well as for a better localization of its seismicity. In the future, it could be planned to extend the Ischia seismic network into areas not covered by seismic stations in order to improve this first 3-D model of the island.

ACKNOWLEDGMENTS

We thank two anonymous Reviewers for constructive and insightful comments that helped to improve the manuscript.

DATA AVAILABILITY

The data underlying this paper will be shared on reasonable request to the corresponding author.

DECLARATION OF COMPETING INTEREST

The authors declare that there is not conflict of interest.

REFERENCES

Acocella, V. & Funiciello, R., 1999. The interaction between regional and local tectonics during resurgent doming: the case of the island of Ischia, Italy, *J. Volc. Geotherm. Res.,* **88,** 109–123.

Agip, 1987. Geologia e geofisica del sistema geotermico dei Campi Flegrei, *Technical report Settore Esplor,* 1–23.

Albarello, D. & Lunedei, E., 2010. Alternative interpretations of horizontal to vertical spectral ratios of ambient vibrations: new insights from theoretical modeling, *Bull. Earthq. Eng.,* **8**(3), 519–534.

Almendros, J., Luzón, F. & Posadas, P., 2004. Microtremor analyses at Teide Volcano (Canary islands, Spain): assessment of natural frequencies of vibration using time-dependent horizontal-to-vertical spectral ratios, *Pure appl. Geophys.,* **161,** 1579–1596.

Bard, P. Y., 1999. Microtremor measurements: a tool for site effect estimation, in *Second International Symposium on the Effects of Surface Geology on seismic motion,* Vol. **3,** pp. 1251–1279, eds Okada & Sasatani, Balkema.

Berrino, G., Corrado, G. & Riccardi, U., 2008. Sea gravity data in the Gulf of Naples. A contribution to delineating the structural pattern of the Phlegraean Volcanic District, *J. Volc. Geotherm. Res.,* **175**. 241–252.

Bonnefoy-Claudet, S., Cornou, C., Yves Bard, P., Cotton, F., Mozco, P., Kristek, J. & Fäh, D., 2006. H/V ratio: a tool for site effects evaluation. Result from 1-D noise simulations, *Geophys. J. Int.,* **167,** 827–837.

Capuano, P., De Matteis, R. & Russo, G., 2015. The structural setting of the Ischia Island caldera (Italy): first evidence from seismic and gravity data, *Bull. Volcanol.,* **77**(9),.

Carlino, S., 2012. The process of resurgence for Ischia Island (southern Italy) since 55Ka: the Laccolith model and implications for eruption forecasting, *Bull. Volcanol.,* **74**(5), 947–961.

Carlino, S., Somma, R., Troiano, A., Di Giuseppe, M.G., Troise, C. & De Natale, G., 2014. The geothermal system of Ischia Island (southern Italy): critical review and sustainability analysis of geothermal resource for electricity generation, *Renew. Ener.,* **62,** 177–196.

de Vita, S., Sansivero, F., Orsi, G. & Marotta, E., 2006. Cyclical slope instability and volcanism related to volcano-tectonism in resurgent calderas: the Ischia island (Italy) case study, *Eng. Geo.,* **86,** 148–165.

Della Seta, M., Marotta, E., Orsi, G., de Vita, S., Sansivero, F. & Fredi, P., 2012. Slope instability induced by volcano-tectonics as an additional source of hazard in active volcanic areas: the case of Ischia island (Italy), *Bull. Volcanol.,* **74,** 79–106.

Di Giuseppe, M.G., Troiano, A. & Carlino, S., 2017. Magnetotelluric imaging of the resurgent caldera on the island of Ischia (southern Italy): inferences for its structure and activity, *Bull. Volcanol.,* **79,** 85.

Dravinski, M., Ding, G. & Wen, K.L., 1996. Analysis of spectral ratio for estimating ground motion in deep basin, *Bull. seism. Soc. Am.,* **86**(3), 646–654.

Ducellier, A., Kawase, H. & Matsushima, S., 2013. Validation of a new velocity structure inversion method based on horizontal-to-vertical (H/V) spectral ratios of earthquake motions in the Tohoku Area, Japan, *Bull. seism. Soc. Am.,* **103**(2A), 958–970.

Fäh, D., Kind, F. & Giardini, D., 2001. A theoretical investigation of average H/V ratios, *Geophys. J. Int.,* **145,** 535–549.

Fäh, D., Kind, F. & Giardini, D., 2003. Inversion of local S-wave velocity structures from average H/V ratios, and their use for the estimation of site-effects, *J. Seismol.,* **7,** 449–467.

Field, E. & Jacob, K., 1993. The theoretical response of sedimentary layers to ambient seismic noise, *Geophys. Res. Lett.,* **20**(24), 2925–2928.

Foti, S. *et al.*, 2018. Guidelines for the good practice of surface wave analysis: a product of the InterPACIFIC project, *Bull. Earthq. Eng.,* **16**(6), 2367–2420.

Galluzzo, D. *et al.*, 2017. Seismic Data acquired by the SISMIKO Emergency Group - Ischia-Italy 2017 - T13 [Data set]. Istituto Nazionale di Geofisica e Vulcanologia (INGV). https://doi.org/10.13127/SD/.

Galluzzo, D. *et al.*, 2019. Le attività del gruppo operativo SISMIKO in occasione del terremoto di Ischia Mw 3.9 (MD 4.0) del 21 Agosto 2017, *Quad. Geofis.,* **154,** 1–28.

García-Jerez, A., Luzón, F., Albarello, D., Lunedei, E., Santoyo, M.A., Margerin, L. & Sánchez-Sesma, F.J., 2012. Comparison between ambient vibrations H/V obtained from the diffuse field and the distributed surface sources models, in *Proceedings of the 15th World Conference on Earthquake Engineering,* IAEE, Lisbon, Portugal.

García-Jerez, A., Luzón, F., Sánchez-Sesma, F.J., Lunedei, E., Albarello, D., Santoyo, M.A. & Almendros, J., 2013. Diffuse elastic wavefield within a simple crustal model. Some consequences for low and high frequencies, *J. geophys. Res.,* **118,** 5577–5595.

Gillot, P.Y., Chiesa, S., Pasquare, G. & Vezzoli, L., 1982. <33.000 yr K -Ar dating of the volcano-tettonic Harst of the Isle of Ischia, Gulf of Naples, *Nature,* **299,** 242–244.

Hobiger, M., Bard, P.Y., Cornou, C. & Le Bihan, N., 2009. Single station determination of Rayleigh wave ellipticity by using the random decrement technique (RayDec), *Geophys. Res. Lett.,* **36,** doi:10.1029/2009GL038863.

Kang, S.Y, Kwang-Hee, K., Jer-Ming, C. & Lanbo, L., 2020. Microtremor HVSR analysis of heterogeneous shallow sedimentary structures at Pohang, South Korea, *J. Geophys. Eng.,* **17,** 861–869.

Kawase, H., Sánchez-Sesma, F.J. & Matsushima, S., 2011. The optimal use of horizontal-to-vertical spectral ratios of earthquake motions for velocity inversions based on diffuse-field theory for plane waves, *Bull. seism. Soc. Am.,* **101**(5), 2001–2014.

Konno, K. & Ohmachi, T., 1998. Ground-motion characteristics estimated from spectral ratio between horizontal and vertical components of microtremor, *Bull. seism. Soc. Am.,* **88**(1), 228–241.

Lachet, C. & Bard, P.Y., 1994. Numerical and theoretical investigations on the possibilities and limitations of Nakamura's technique, *J. Phys. Earth.,* **42,** 377–397.

Lunedei, E. & Albarello, D., 2010. Theoretical HVSR curves from full wavefield modelling of ambient vibrations in a weakly dissipative layered Earth, *Geophys. J. Int.,* **181,** 1093–1108.

Lunedei, E. & Albarello, D., 2015. Horizontal-to-vertical spectral ratios from a full-wavefield model of ambient vibrations generated by a distribution of spatially correlated surface sources, *Geophys. J. Int.,* **201,** 1142–1155.

Lunedei, E. & Malischewsky, P., 2015. A review and some new issues on the theory of the H/V technique for ambient vibrations, in *Perspectives on European Earthquake Engineering and Seismology. Geotechnical, Geological and Earthquake Engineering,* Vol. **39,** pp. 371–394, Ansal, A., Springer.

Luzón, F., Al Yuncha, Z., Sánchez-Sesma, F.J. & Ortiz-Aleman, C., 2001. A numerical experiment on the horizontal to vertical spectral ratio in flat sedimentary basins, *Pageoph,* **158,** 2451–2461.

Maghami, S., Sohrabi-Bidar, A., Bignardi, S., Zarean, A. & Kamalian, M., 2021. Extracting the shear wave velocity structure of deep alluviums of "Qom" basin (Iran) employing HVSR inversion of microtremor recordings, *J. appl. Geophys.,* **185,** 104246.

Malischewsky, P.G. & Scherbaum, F., 2004. Love's formula and H/V-ratio ellipticity of Rayleigh waves, *Wave Motion,* **40,** 57–67.

Maresca, R., Nardone, L., Pasquale, G., Pinto, F. & Bianco, F., 2012. Effects of surface geology on seismic ground motion deduced from ambient-noise measurements in the town of Avellino, Irpinia Region (Italy), *Pure appl. Geophys.,* **169,** 1173–1188.

Martorana, R., Agate, M., Capizzi, P., Cavera, F. & D'Alessandro, A., 2018. Seismo-stratigraphic model of "La Bandita" area in the Palermo Plain (Sicily, Italy) through HVSR inversion constrained by stratigraphic data, *Ital. J. Geosci.,* **137,** 73–86.

Martorana, R., Capizzi, P., Avellone, G., Siragusa, R., D'Alessandro, A. & Luzio, D., 2017. Assessment of a geological model by surface wave analyses, *J. Geophys. Eng.,* **14**(1), 159–172.

Molnar, S. *et al.*, 2022. A review of the microtremor horizontal-to-vertical spectral ratio (MHVSR) method, *J. Seismol,* 1–33 https ://doi.org/10.1007/s10950-021-10062-9.

Mucciarelli, M., Contri, P., Monachesi, G., Galvano, G. & Gallipoli, M.R., 2001. An empirical method to asses the seismic vulnerability of existing building usind the HVSR technique, *Pure appl. Geophys.,* **158,** 2635–2647.

Mucciarelli, M., Gallipoli, M.R. & Arcieri, M., 2003. The stability of horizontal-to-vertical spectral ratio by triggered noise and earthquake recordings, *Bull. seism. Soc. Am.,* **93,** 1407–1412.

Nakamura, Y., 1989. Method for dynamic characteristics estimation of subsurface using microtremor on the ground surface, *Quart. Rep. RTRI (Railway Technical Research Institute) (Japan),* **30**(1), 25–33.

Nakamura, Y., 2000. Clear identification of fundamental idea of Nakamura's technique and its applications.

Napolitano, F., Gervasi, A., La Rocca, M., Guerra, I. & Scarpa, R., 2018. Site effects in the Pollino Region from the HVSR and polarization of seismic noise and earthquakes, *Bull. seism. Soc. Am.,* **108**(1), 309–321.

Nardone, L., Esposito, R., Galluzzo, D., Petrosino, S., Cusano, P., La Rocca, M., Di Vito, M.A. & Bianco, F., 2020a. Array and spectral ratio applied to seismic noise to investigate the Campi Flegrei (Italy) subsoil structure at different scales, *Adv. Geosci.,* **52,** 75–85.

Nardone, L., Manzo, R., Galluzzo, D., Pilz, M., Carannante, S., Di Maio, R. & Orazi, M., 2020b. Shear wave velocity and attenuation structure of Ischia island using broad band seismic noise records, *J. Volc. Geotherm. Res.,* **401**(106970), 1–13.

Nogoshi, M. & Igarashi, T., 1970. On the amplitude characteristics of microtremors, *J. Seismol. Soc. Jpn.,* **23,** 264–280.

Nogoshi, M. & Igarashi, T., 1971. On the amplitude characteristics of microtremor (Part 2), *J. Seismol. Soc. Jpn.,* **24,** 26–40.

Okada, H., 2003. The microtremor survey methods, Geophys. Monogr. No. 12, SEG.

Orazi, M. *et al.*, 2018. La rete sismica di Ischia dell'Osservatorio Vesuviano – INGV: evoluzione, configurazione attuale e performance, in *Proceedings of the 37° GNGTS,* pp. 261–265.

Orsi, G., Gallo, G. & Zanchi, A., 1991. Simpleshearing block resurgence in caldera depressions. A model from Pantelleria and Ischia, *J. Volc. Geotherm. Res.,* **47,** 1–11.

Özalaybey, S., Zor, E., Ergintav, S. & Tapirdamaz, M. C., 2011. Investigation of 3-D basin structures in the İzmit Bay area (Turkey) by single-station microtremor and gravimetric methods, *Geophys. J.Int.,* **186**. 883–894.

Panzera, P., Sicali, S., Lombardo., G., Imposa, S., Gresta, S. & D'Amico, S., 2016. A microtremor survey to define the subsoil structure in a mud vulcanoes area: the case study of Salinelle (Mt. Etna, Italy), *Environ. Earth Sci.,* **75,** 1140.

Paoletti, V. *et al.*, 2009. The Ischia volcanic island (southern Italy): inferences from potential field data interpretation, *J. Volc. Geotherm. Res.,* **179,** 69–86.

Paoletti, V., Fedi, M. & Florio, G., 2017. The structure of the Ischia Volcanic Island from magnetic and gravity data, *Ann. Geophys.,* **60,** Supplement to 6, GM674, 2017; doi: 10.4401/ag-7550.

Penta, F., 1963. Sulle caratteristiche idrotermologiche dell'isola d'Ischia (Napoli), *Rend. Acc. Lincei.,* **34,** 1–8.

Penta, F. & Conforto, B., 1951. Risultati di sondaggi e di ricerche geominerarie nell'isola d'Ischia dal 1939 al 1943, nel campo del vapore, delle acque termali e delle "forze endogene" in generale", *Ann Geophys.*, **4,** 159–191.

Picotti, S., Francese, R., Giorgi, M., Pettenati, F. & Carcione, J.M., 2017. Estimation of glaciers thicknesses and basal properties using the horizontal-to-vertical component spectral ratio (HVSR) technique from passive seismic data, *J. Glaciol,* **63,** 229–248.

Pilz, M., Parolai, S., Picozzi, M., Wang, R., Leyton, F., Campos, J. & Zschau, J., 2010. Shear wave velocity model of the Santiago de Chile basin derived

from ambient noise measurements: a comparison of proxies for seismic site conditions and amplification, *Geophys. J. Int.,* **182**. 355–367.

Poggi, V. & Fäh, D., 2010. Estimating Rayleigh wave particle motion from three-component array analysis of ambient vibrations, *Geophys. J. Int.,* **180**. 251–267.

Rittmann, A., 1930. Geologie der Insel Ischia. Z. F. Vulkanol. Ergänzungsband. 6.

Sánchez-Sesma, F. J. *et al.*, 2011. A theory for microtremor H/V spectral ratio: application for a layered medium, *Geophys. J. Int.,* **186,** 221–225.

Sbrana, A., Fulignati, P., Marianelli, P.C., Boyce, A.J. & Cecchetti, A., 2009. Exhumation of an active magmatic-hydrothermal system in a resurgent caldera environment: the example of Ischia (Italy), *J. Geol. Soc.,* **166**(6), 1061–1073.

Sbrana, A., Marianelli, P. & Pasquini, G., 2018. Volcanology of Ischia (Italy), *J. Maps.,* **14**(2), 494–503.

Sbrana, A. & Toccaceli, R.M., 2011. Carta Geologica della Regione Campania – Foglio 464 – Isola di Ischia, Progetto CARG Regione Campania – Assessorato Difesa del Suolo, Litografia Artistica Cartografica, Firenze.

Strollo, R., Nunziata, C., Iannotta, A. & Iannotta, D., 2015. The uppermost crust structure of Ischia (southern Italy) from ambient noise Rayleigh waves. *J. Volc. Geotherm. Res.,* **297,** 39–51.

Tokimatsu, K., 1995. Geotechnical site characterization using surface waves, in *Earthquake Geotechnical Engineering,* pp. 1333–1368, ed. Ishihara, Balkema.

Torrese, P.,Rossi, A.P.,Unnithan, V.,Pozzobon, R.,Borrmann, D.,Lauterbach, H.,Luzzi, E.& Sauro, F..2020. HVSR passive seismic stratigraphy for the investigation of planetary volcanic analogues, *Icarus* **351**().

Villaseñor, A.P., 2010. *Physical and mechanical characterization of altered volcanic rocks for the stability of volcanic edifices, PhD thesis*, University of Milan – Bicocca, Milan, Italy.

Wathelet, M., Chatelain, J.C., Cornou, C., Di Giulio, G., Guillier, B., Ohrnberger, M. & Savvaidis, A., 2020. Geopsy: a user-friendly open-source tool set for ambient vibration processing, *Seismol. Res. Lett.,* **91**(3), 1878–1889.

Wathelet, M., Jongmans, D. & Ohrnberger, M., 2004. Surface-wave inversion using a direct search algorithm and its application to ambient vibration measurements, *Near Surf. Geophys.,* **2**(22), 211–221.

Wathelet, M., Jongmans, D. & Ohrnberger, M., 2005, Direct inversion of spatial autocorrelation curves with the neighbourhood algorithm, *Bull. seism. Soc. Am.,* **95**(5), 1787–1800.

Wathelet, M., Jongmans, D., Ohrnberger, M. & Bonnefoy-Claudet, S., 2008. Array performances for ambient vibrations on a shallow structure and consequences over Vs inversion, *J. Seismol.,* **12,** 1–19.